Modeling and Optimization of Magnetically Coupled Resonant Wireless Power Transfer System With Varying Spatial Scales

Fuxin Liu, *Senior Member, IEEE*, Yong Yang, Dan Jiang, Xinbo Ruan, *Fellow, IEEE*, and Xuling Chen, *Student Member, IEEE*

***Abstract*—Previous work reveals that the magnetically coupled resonant (MCR) wireless power transfer (WPT) technology is efficient and practical for mid-range wireless energy transmission, able to handle nontrivial amount of power. Due to the variable coupling coefficient under lateral misalignment and angular misalignment between transmitting coils and receiving coils, the output power and transmission efficiency will fluctuate, leading to instability of the system. This paper presented an equivalent analytical model for the MCR WPT system to incorporate spatial misalignments. The mutual inductance formulas were derived when receiving coils are laterally, angularly or generally misaligned from transmitting coils. The relationship among the output power, transmission efficiency, the mutual inductance, and load resistance were analyzed in detail. For the design of the MCR WPT system, it is necessary to seek optimal transmission performance under different applications. To achieve maximum output power and high stability of power transfer in a specific misalignments range, a normalization method based on the obtained analytical model was introduced, providing critical insight into the optimal design of coils. Relative design considerations and optimization procedures were further stated. Experiments had also been carried out to evaluate the accuracy of theoretical analysis and confirm the validity of the proposed optimization method.**

***Index Terms*—Angular misalignment, lateral misalignment, magnetically coupled resonant (MCR), spatial scales, wireless power transfer (WPT).**

I. Introduction

WIRELESS power transfer (WPT) is a promising technology to be applied in many fields, such as electric vehicles, consumer electronics, and implantable medical devices, due to its superiority on convenience of being cordless, safety during power charging, and ability to operate in wet and harsh environment [1]–[4]. Recently, magnetically coupled inductive (MCI) WPT and magnetically coupled resonant (MCR) WPT are two popular techniques of WPT [5]. Some MCI WPT cases have exhibited high power transmission efficiency, normally larger than 90% for several centimeters transmission distance [6]. But, once the distance gets longer, the efficiency will drop significantly. MCR WPT is a near-field WPT technique for mid-range (10–300 cm). In 2007, scientists in Massachusetts Institute of Technology made a breakthrough in such advanced field, successfully lighting up a 60 W bulb over distances in excess of 2 m [7]. The follow-up studies have shown that MCR WPT provides higher efficiency in longer transmission distance compared to MCI WPT [8]. Therefore, it is considered to be one of the most potential techniques for mid-range WPT applications at present.

In the MCR WPT system, the transmitting coils and receiving coils are designed to resonate at the operating frequency, establishing an efficient energy channel for power transfer. Previous work mainly focused on how to enhance transmission efficiency for longer distance when Transmitter and receiver are perfectly aligned along a fixed axis. Many ways to improve transmission efficiency had been proposed, such as introducing the intermediate resonant coils [9], realizing soft switching for power devices [10], optimizing the structure and parameters of coils [11], etc. However, in some applications such as medical implants, charging device for mobile phones, etc., the spatial scales of coils including transmission distance, lateral misalignment, and angular misalignment, may vary randomly under different environment. The varying spatial scales of coils will alter the mutual inductance, further cause fluctuations in output power and transmission efficiency. So, it is critical to be able to predict the misalignment tolerance of such system and specify the geometric boundaries of steady operation. In [12], a lucid approach was presented for the mutual inductance calculation in various misalignment cases, but the misalignment effects on transmission characteristics were not discussed. In [13], the lateral misalignment was investigated and high efficiency range was identified, but without considering coil orientation. A novel analytical model for the MCR WPT system was proposed in [14], which incorporates coil misalignment when analyzing the output voltage and transmission efficiency using the finite-element method. In [15], coil orientation was directly integrated into the calculation of transmission efficiency, avoiding involving the mutual inductance. However, the general misalignment case in which lateral displacement and

Manuscript received December 18, 2015; revised March 14, 2016 and April 28, 2016; accepted June 2, 2016. Date of publication June 22, 2016; date of current version January 20, 2017. This paper was presented in part at the *IEEE Energy Conversion Congress and Exposition, 2015*, and at the *IEEE Applied Power Electronics Conference and Exposition, 2016*. This work was supported by grants from the Natural Science Foundation of China under Award 51505223, by the Natural Science Foundation of Jiangsu Province, China, under Award BK20151471, by the Lite-on Research Program, and by the Jiangsu Province University Outstanding Science and Technology Innovation Team Project. Recommended for publication by Associate Editor S. Y. Hui.

F. Liu, Y. Yang, D. Jiang, and X. Ruan are with the Jiangsu Key Laboratory of New Energy Generation and Power Conversion, College of Automation Engineering, Nanjing University of Aeronautics and Astronautics, Nanjing 210016, China (e-mail: liufuxin@nuaa.edu.cn; yangyong_nuaa@126.com; xiaobai_bingo@nuaa.edu.cn; ruanxb@nuaa.edu.cn).

X. Chen is with the College of Mechanical and Electrical Engineering, Nanjing University of Aeronautics and Astronautics, Nanjing 210016, China (e-mail: chenxuling@nuaa.edu.cn).

Color versions of one or more of the figures in this paper are available online at http://ieeexplore.ieee.org

Digital Object Identifier 10.1109/TPEL.2016.2581840

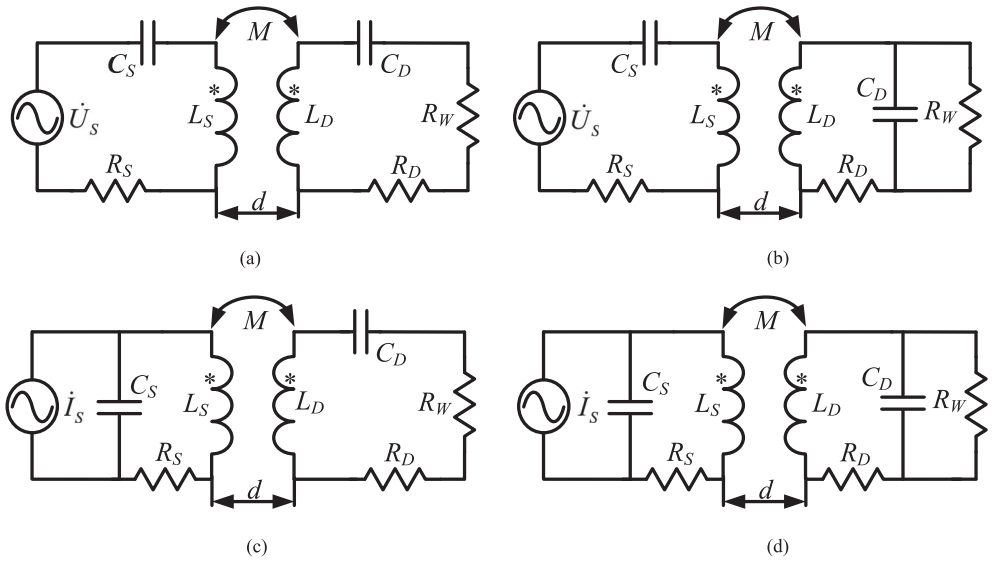

Fig. 1. Four basic compensation topologies. (a) SS. (b) SP. (c) PS. (d) PP.

angular tilt of coils occur simultaneously was considered in neither [14] nor [15].

Meanwhile, for the design of the MCR WPT system, it is crucial to seek optimal transmission performance under different specifications. In [16], optimum design of the two-coil coupler was discussed and the impact of coil parameters on the transmission efficiency was emphatically analyzed. In [17], low coupling coefficient was thought to be the dominant factor that results in difficulties to achieve high efficiency or large amount of power transfer, so it proposed a method to improve the coupling coefficient by optimizing the structure of coils. Deficiently, neither studies in [16] nor [17] took spatial misalignments into account. In [18], a novel power transfer function was introduced which combines coil spatial misalignments with several key parameters of the system in deducing the relationship among the transmission efficiency. Unfortunately, none of these researches developed a systematic design procedure to guide the selection of optimal parameters for a desired output power.

This paper focused on the modeling of the MCR WPT system with varying spatial scales. The equivalent circuit of the system consisting of a half-bridge inverter and a voltage-doubler rectifier was derived, according to the fundamental harmonic analysis (FHA) method. Based on the equivalent circuit, expressions of the output power and transmission efficiency were deduced. Further, the corresponding mutual inductance formulas were also derived. Meanwhile, a detailed theoretical analysis of misalignment effects on transmission characteristics with varied load was presented, including lateral misalignment, angular misalignment, and general misalignment. By normalizing mutual inductance into a function only related to coil turns and solving the differential equation of output power, the steady operation range and optimum value of coil turns to achieve maximum power transfer were obtained. Finally, a prototype had been built and tested to validate the theoretical analysis.

II. Description of the MCR WPT System

To enhance the capacity of power transfer, improve the system efficiency, and lower the voltage and current stress of source and load, resonances need to be ensured in both the transmitting side and the receiving side [19]. To meet such requirement, the resonant capacitors should be introduced for power compensation. Four basic compensation topologies labeled as SS, SP, PS, and PP are shown in Fig. 1, where the first S or P indicates series or parallel compensation for transmitting coils and the second S or P means series or parallel compensation for receiving coils. In Fig. 1, L_S and L_D are the resonant inductors. C_S and C_D are the resonant capacitors. M is the mutual inductance. d is the transmission distance. R_W is the equivalent load resistance. R_S and R_D are the parasitic resistances of coils. Here, resonant capacitors C_S and C_D can be provided not only by external capacitors but also by parasitic capacitances of the coils. According to the compensation configuration, the transmitting coils can be driven either by ac voltage source or by ac current source.

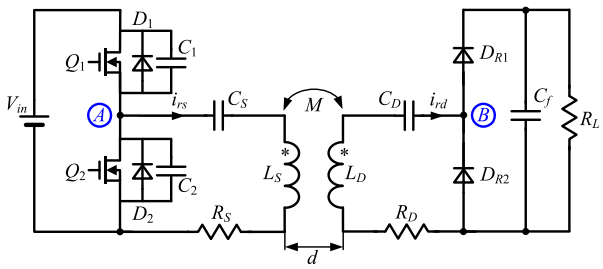

Fig. 2. Topology configuration of the MCR WPT system.

Among the four basic compensation topologies, only the equivalent reactance of SS topology looking from the power source is independent of the mutual inductance, resonant inductors or the load resistance at the resonant frequency. Therefore, this paper selects the SS topology for the following discussion and adds external capacitors to act as the resonant capacitors. In general, the values of coil parasitic capacitances are so smaller than those of added external capacitors that can be ignored in analysis.

Fig. 2 shows the topology configuration of the MCR WPT system researched in this paper. As shown, the resonant tank is driven by a half-bridge inverter with dc input voltage and the

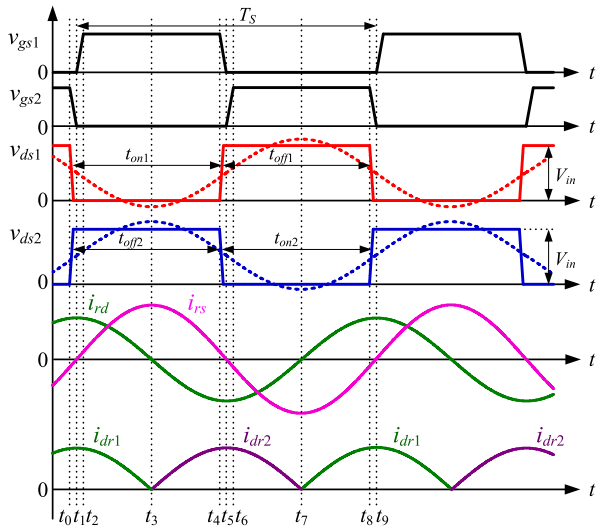

Fig. 3. Key waveforms of the MCR WPT system.

output voltage is rectified by a voltage-doubler rectifier. Fig. 3 depicts the key voltage and current waveforms of the system. $v_{\rm gs1}$ and $v_{\rm gs2}$ are the gate-drive voltages of power switches. $v_{\rm ds1}$ and $v_{\rm ds2}$ are the drain-to-source voltages of them. $i_{\rm rs}$ and $i_{\rm rd}$ are the resonant currents of transmitting coils and receiving coils respectively. $i_{\rm dr1}$ and $i_{\rm dr2}$ are the currents flowing through the rectifier diodes. The dashed lines represent the fundamental harmonic of the square-wave voltage.

From Fig. 3, it can be known that two power switches are turned on or off alternately with a small dead time for soft switching. During the dead time, the parasitic capacitance of the power switch is discharged by the lagged resonant current in case of inductive impedance condition. Before the power switches turns on, the drain-to-source voltage is clamped at zero, resulting in no turned-on loss. Thus, the power switches can realize zero-voltage switching (ZVS). Meanwhile, the currents of rectifier diodes are naturally decreased to zero when they are turned off, which means the rectifier diodes can operate with zero-current switching (ZCS). Both ZVS and ZCS operation are beneficial for high power efficiency and low electromagnetic interference noise, especially in high frequency application.

III. Modeling and Analysis of Transmission Characteristics

Generally, the quality factors of resonant coils in the WPT system are very high and the resonant currents are almost sinusoidal waveforms. So, FHA can be adopted for the steady-state analysis, which only considers the fundamental component and neglects the dc component or higher harmonics. The equivalent circuit of the system based on FHA is shown in Fig. 4. Phasor $\dot{U}_S$ is the fundamental harmonic of the ac voltage applied on the transmitting coils. Phasors $\dot{I}_S$ and $\dot{I}_D$ are the fundamental harmonics of the resonant currents.

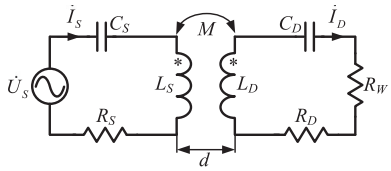

Fig. 4. Equivalent circuit of the MCR WPT system.

In order to simplify the analysis, the following assumptions are made:

1) resonant inductor $L_S = L_D$, resonant capacitor $C_S = C_D$;
2) parasitic resistance of coils $R_S = R_D$, which are assumed to be constant.

A. Output Power and Transmission Efficiency

Due to the half-bridge configuration, the norm of $\dot{U}_S$ can be calculated as

$$U_S = \left\|\dot{U}_S\right\| = \frac{\sqrt{2}}{\pi} V_{\rm in}. \tag{1}$$

The relationship between the equivalent load resistance R_W and the real load resistance R_L is

$$R_W = \frac{2}{\pi^2} R_L. \tag{2}$$

According to the equivalent circuit shown in Fig. 4 and Kirchhoff voltage law, we can obtain

$$\begin{bmatrix} \dot{U}_S \\ 0 \end{bmatrix} = \begin{bmatrix} R_S + jX_S & -j\omega M \\ -j\omega M & R_D + R_W + jX_D \end{bmatrix} \cdot \begin{bmatrix} \dot{I}_S \\ \dot{I}_D \end{bmatrix} \tag{3}$$

where X_S and X_D are equivalent reactances of the transmitter and receiver, respectively,

$$X_S = \omega L_S - \frac{1}{\omega C_S}, \quad X_D = \omega L_D - \frac{1}{\omega C_D}. \tag{4}$$

Assuming $Z_S = R_S + jX_S$ and $Z_D = R_D + R_W + jX_D$, $\dot{I}_S$ and $\dot{I}_D$ can easily be solved from the previous equations

$$\dot{I}_S = \frac{\dot{U}_S}{Z_S + (\omega M)^2 / Z_D} \tag{5}$$

$$\dot{I}_D = \frac{j\omega M}{Z_D} \dot{I}_S. \tag{6}$$

Therefore, the output power of the system is (7) shown at the bottom of the page.

Assuming that the radiation loss and power losses are negligible, the transmission efficiency of the system can be expressed

$$P_O = {I_D}^2 R_W = \frac{{U_S}^2 \cdot (\omega M)^2 R_W}{\left[R_S (R_D + R_W) - X_S X_D + (\omega M)^2\right]^2 + \left[R_S X_D + (R_D + R_W) X_S\right]^2} \tag{7}$$

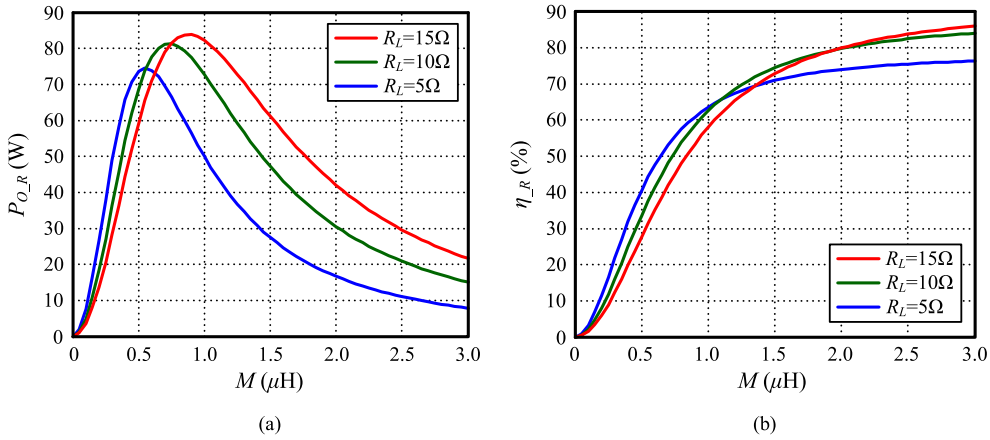

Fig. 5. Transmission characteristics versus mutual inductance. (a) Output power. (b) Transmission efficiency.

as

$$\eta = \frac{{I_D}^2 R_W}{{I_S}^2 R_S + {I_D}^2 (R_D + R_W)} = \frac{(\omega M)^2 R_W}{R_S \left[(R_D + R_W)^2 + {X_D}^2\right] + (\omega M)^2 (R_D + R_W)}. \tag{8}$$

From (7) and (8), it can be seen that the output power of the system depends on both X_S and X_D, while the transmission efficiency of the system is independent on X_S.

The resonant frequency of the MCR WPT system is defined as

$$f_r = 1/\left(2\pi\sqrt{L_r C_r}\right). \tag{9}$$

When the transmitting coils and receiving coils are both designed to resonate at the operating frequency, we can get $X_S = X_D = 0$. Then, (7) and (8) can be simplified as

$$P_{O\_R} = \frac{{U_S}^2 \cdot (\omega M)^2 R_W}{\left[R_S (R_D + R_W) + (\omega M)^2\right]^2} \tag{10}$$

$$\eta_{\_R} = \frac{(\omega M)^2 R_W}{R_S (R_D + R_W)^2 + (\omega M)^2 (R_D + R_W)}. \tag{11}$$

Equations (1), (2), (10), and (11) show that P_{O_R} and $\eta_{\_R}$ are both the function of the mutual inductance M and load resistance R_L. Fig. 5 illustrates the curves of P_{O_R} and $\eta_{\_R}$ with various M and R_L, which indicate that the mutual inductance and load resistance will affect the transmission characteristics significantly. The specifications are listed as follows: $V_{\text{in}} = 24$ V,$\text{f}_\text{s} = 202$ kHz,$\text{R}_\text{S} = \text{R}_\text{D} = 0.28\ \Omega$.

B. Mutual Inductance With Varying Spatial Scales

The varying spatial scales of transmitting and receiving coils will alter the mutual inductance, further affect the output power and transmission efficiency. To describe the relationship between the transmission characteristics and the spatial scales directly, it is important to obtain the mutual inductance formulas in arbitrary spatial scales. This can be realized by solving the double integral in Neumann's formula

$$M = \frac{N_S N_D \mu_0}{4\pi} \times \oint \oint \frac{\mathbf{dl_S} \cdot \mathbf{dl_D}}{r_{\text{SD}}} \tag{12}$$

where $N_S, \text{N}_\text{D}, \text{l}_\text{S}, \text{l}_\text{D}, \mathbf{dl_S}$, and $\mathbf{dl_D}$ are, respectively, the coil turns, the length of each turn and the infinitesimal of l of transmitting coils and receiving coils. r_{SD} is the distance between $\mathbf{dl_S}$ and $\mathbf{dl_D}$. μ_0 is the magnetic permeability of vacuum. For clarity, we only show the case of one-turn coil in next diagrams. According to different spatial scales, the coil configurations can be classified into four cases, as illustrated in Fig. 6.

The most complicated general case shown in Fig. 6(d) will be analyzed first, where both lateral and angular misalignments are included. The others are just special cases derived from it. The line elements $\mathbf{dl_S}$ and $\mathbf{dl_D}$, and the distance r_{SD} can be evaluated by geometrical methods

$$\mathbf{dl_S} = r_S\,(-\sin\theta\mathbf{x} + \cos\theta\mathbf{y})\,d\theta \tag{13}$$

$$\mathbf{dl_D} = r_D\,(-\sin\phi\cos\alpha\mathbf{x} + \cos\phi\mathbf{y} + \sin\phi\sin\alpha\mathbf{z})\,d\phi \tag{14}$$

$$r_{\text{SD}} = \left[r_S^2 + r_D^2 + d^2 + \Delta^2 + 2\Delta r_D\cos\phi\cos\alpha - 2\Delta r_S\cos\theta - 2r_S r_D(\cos\theta\cos\phi\cos\alpha + \sin\theta\sin\phi) - 2r_D d\cos\phi\sin\alpha\right]^{\frac{1}{2}}. \tag{15}$$

Substituting (13)–(15) into (12) yields

$$M_G = \frac{N_S N_D \mu_0 r_S r_D}{4\pi} \times \oint d\phi \oint \frac{\sin\theta\sin\phi\cos\alpha + \cos\theta\cos\phi}{r_{\text{SD}}} d\theta. \tag{16}$$

Referring to (16), other cases can be analyzed as follows:

1) In the ideal alignment case shown in Fig. 6(a), two parallel coils are coaxial, so $\Delta = 0$ cm and $\alpha = 0^\circ$

$$M_I = \frac{N_S N_D \mu_0 r_S r_D}{4\pi} \times \oint d\phi \oint \frac{\sin\theta\sin\phi + \cos\theta\cos\phi}{r_{\text{SD}}} d\theta \tag{17}$$

where

$$r_{\text{SD}} = \left[{r_S}^2 + {r_D}^2 + d^2 - 2r_S r_D(\cos\theta\cos\phi + \sin\theta\sin\phi)\right]^{\frac{1}{2}}. \tag{18}$$

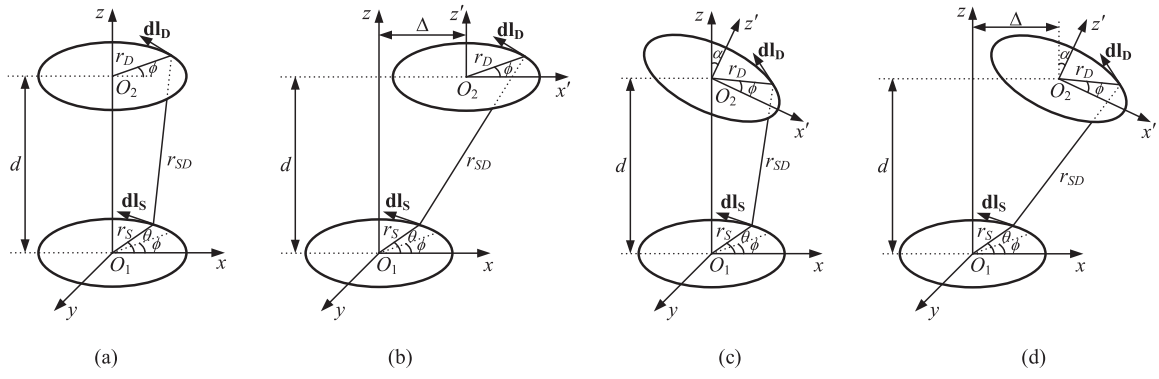

Fig. 6. Coil configurations with various spatial scales. (a) Ideal alignment. (b) Lateral misalignment. (c) Angular misalignment. (d) General misalignment.

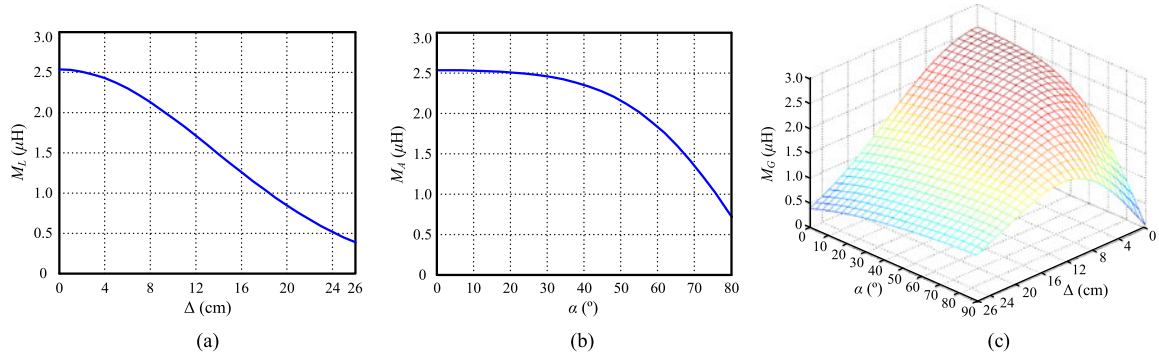

Fig. 7. Mutual inductance with different misalignments. (a) Lateral misalignment case. (b) Angular misalignment case. (c) General misalignment case.

2) In the lateral misalignment case shown in Fig. 6(b), two coils are still in parallel planes but their centers are misplaced by a distance Δ, so only $\alpha = 0°$

$$M_L = \frac{N_S N_D \mu_0 r_S r_D}{4\pi} \times \oint d\phi \oint \frac{\sin\theta \sin\phi + \cos\theta \cos\phi}{r_{\mathrm{SD}}} d\theta \quad (19)$$

where

$$r_{\mathrm{SD}} = \left[{r_S}^2 + {r_D}^2 + d^2 + \Delta^2 + 2\Delta r_D \cos\phi - 2\Delta r_S \cos\theta - 2 r_S r_D (\cos\theta \cos\phi + \sin\theta \sin\phi)\right]^{\frac{1}{2}}. \quad (20)$$

3) In the angular misalignment case shown in Fig. 6(c), the planes of two coils are tilted with an angle α and the axis of one coil passes through the center of the other coil, so only $\Delta = 0$ cm

$$M_A = \frac{N_S N_D \mu_0 r_S r_D}{4\pi} \times \oint d\phi \oint \frac{\sin\theta \sin\phi \cos\alpha + \cos\theta \cos\phi}{r_{\mathrm{SD}}} d\theta \quad (21)$$

where

$$r_{\mathrm{SD}} = \left[{r_S}^2 + {r_D}^2 + d^2 - 2 r_D d \cos\phi \sin\alpha - 2 r_S r_D (\cos\theta \cos\phi \cos\alpha + \sin\theta \sin\phi)\right]^{\frac{1}{2}}. \quad (22)$$

Based on (16), (19), and (21), Fig. 7 shows the mutual inductance curves against the lateral, angular, and general misalignment, respectively. The specifications are listed as follows: $V_{\mathrm{in}} = 24$ V, $\mathrm{f_s} = 200$ kHz, $\mathrm{R_L} = 10\ \Omega$, $\mathrm{r_S} = \mathrm{r_D} = 11$ cm, $\mathrm{N_S} = \mathrm{N_D} = 14$, $\mathrm{d} = 24$ cm. Substituting the obtained mutual inductance formulas into (10) and (11), the relationship between the transmission characteristics and the spatial scales can be revealed, which is as depicted in Fig. 8.

IV. Parameter Optimization of Coils to Achieve Maximum Power

As indicated above, the transmission performance of the MCR WPT system is sensitive to coil spatial misalignments. From Fig. 8, it can be observed that output power varies in an unpredictable manner when receiving coils are laterally or angularly misaligned from transmitting coils. So, it is desirable to optimize the system to improve the transmission stability. This paper focused on the optimal design of coil parameters to achieve maximum power transfer by using a normalization method. According to different specifications, it can be classified into three cases: 1) both the transmitting coils and receiving coils are flexible to design; 2) when the dimension of transmitting coils is mechanically fixed, only receiving coils are allowed to be optimized; and 3) when the redesign of receiving coils is forbidden, only transmitting coils can be modified. As the analysis processes of three cases are similar, for simplicity, we just take case 1 as a example for discussion.

Assuming the transmitting coils and receiving coils are identical helical coils employing the same way of winding with

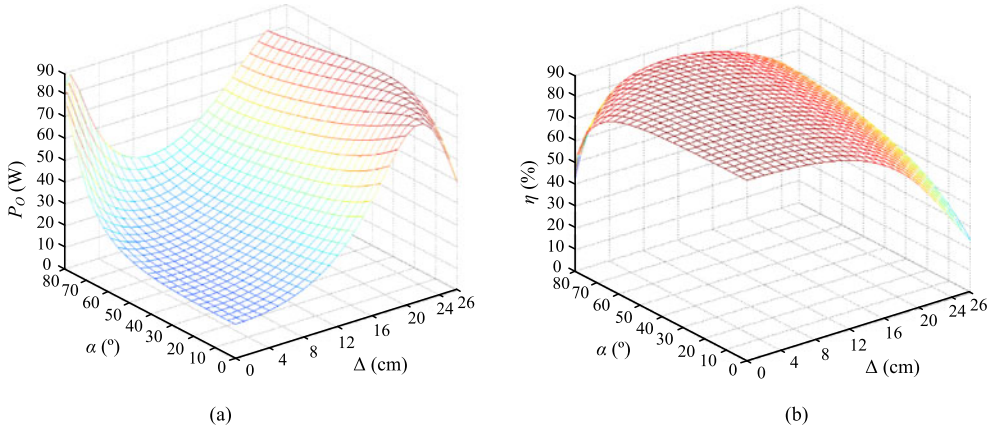

Fig. 8. Three-dimensional view of transmission charactersitics under different spatial scales. (a) Output power. (b) Transmission Efficiency.

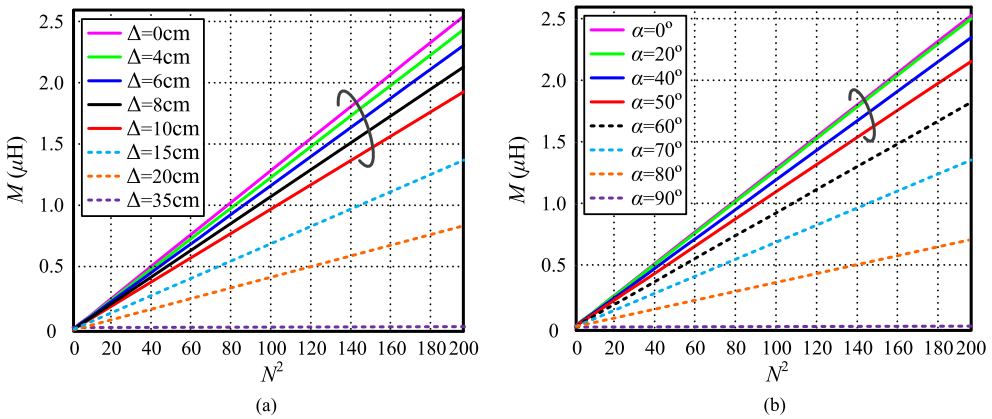

Fig. 9. Mutual inductance with spatial misalignments in case 1. (a) Lateral misalignment. (b) Angular misalignment.

same parameters: $N_S = N_D = N, \mathrm{r_S} = \mathrm{r_D} = \mathrm{r}, \mathrm{R_S} = \mathrm{R_D} = \mathrm{R}$, then (16) can be simplified as

$$M_1 = \frac{\mu_0 N^2 r^2}{4\pi} \oint d\phi \oint \frac{\sin\theta \, \sin\phi \, \cos\alpha + \cos\theta \, \cos\phi}{r_{\mathrm{SD}}} d\theta. \tag{23}$$

Based on (23), there are two variables (coil radius and coil turns) that can be optimized. For specific applications, the coil radius is always dimensionally determined, so we preset it as a constant and normalize the mutual inductance into a function only related to coil turns

$$M_1 = x_1(\Delta, \alpha) \cdot N^2 \tag{24}$$

where $x_1(\Delta,\alpha)$ is a variable coefficient depending on the lateral misalignment Δ and angular misalignment α.

Fig. 9 illustrates the mutual inductances against the square of coil turns with various spatial misalignments. From Fig. 9, it can be seen that the mutual inductance almost increases linearly following the growth of the square of coil turns. The slope remains almost unchanged within the misalignments range of 0–10 cm and 0–50°. The average value of the slope $(0 - 10\ \mathrm{cm}, 0 \sim 50°)$ is calculated to be 1.20×10^{-8}. We use this calculated result to replace $x_1(0 \sim 10\ \mathrm{cm}, 0 \sim 50°)$ in further analysis. Here, the specifications are as follows: $r = 11$ cm,d $= 24$ cm.

From (10), it is known that P_{O} is also related to the parasitic resistances of coils, which are mainly composed of the ac component. Generally, ac losses of coils in the resonant system consist of ohmic (R_o) loss inside the coils and radiative loss (R_r) into free space. At low frequencies, it is dominated by ohmic loss and at high frequencies by radiation. With the operation frequency of hundreds of kilohertz in this paper, R_r is in the order of magnitude of 10^{-4} Ω, that is so smaller than R_o that can be ignored. Thus, for a coil with *N* turns and made of a material with conductivity σ, ac loss resistance R_{ac} can be expressed as [7]

$$R_{\mathrm{ac}} = \sqrt{\frac{\omega\mu_0}{2\sigma}} \cdot \frac{l}{2\pi a} \tag{25}$$

where *l* and *a* are, respectively, the total length and the cross-sectional radius of the wire, and ω is the operating angular frequency. For tightly wound identical helical coils, the total length can be expressed as

$$l = 2\pi \cdot N \cdot r. \tag{26}$$

Substituting (26) into (25) yields

$$R_{\mathrm{ac}} = \frac{1}{a}\sqrt{\frac{\omega\mu_0}{2\sigma}} \cdot N \cdot r. \tag{27}$$

As the material of resonant coils in the MCR WPT system is multistrand litz wire, we modify the formula of R_{ac}

$$R_{\mathrm{ac}} = \frac{1}{nr_a}\sqrt{\frac{\omega\mu_0}{2\sigma}} \cdot N \cdot r \tag{28}$$

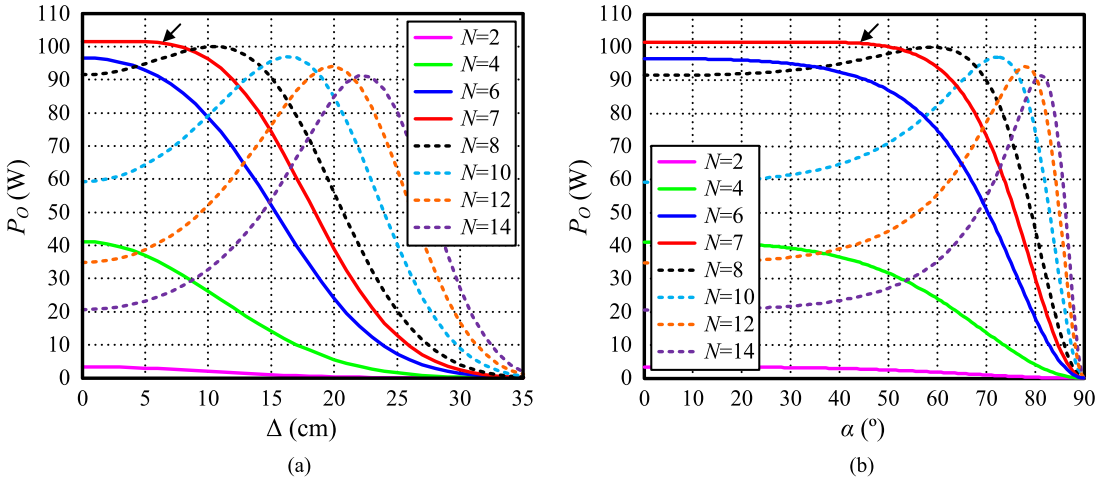

Fig. 10. Output power with spatial misalignments in case 1. (a) Lateral misalignment. (b) Angular misalignment.

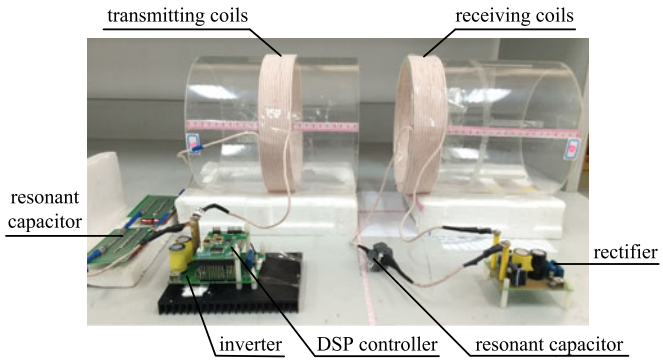

Fig. 11. Prototype of the MCR WPT system.

where n and r_a are, respectively, the number of strands and single-strand radius of the wire.

For the litz wire used in this paper, we found that the measured $R_{\rm ac}$ presents larger than the theorectical value. Reffering to the measured data, a compensated term relative to the turns $R_{\rm comp}$ is introduced and the parasitic resistance of coils can be given by

$$R = R_{\rm comp} + R_{\rm ac} = \left(k_{\rm comp} + \frac{r}{nr_a}\sqrt{\frac{\omega\mu_0}{2\sigma}}\right)\cdot N \tag{29}$$

where $k_{\rm comp}$ is a constant, which is equal to 0.015 by matching the measured data. It also should be noted that $k_{\rm comp}$ is frequency dependent, and is acquired at the frequency of hundreds of Hertz. As σ,n,$\rm r_a$, and ω are a set of given parameters, following the normalization method above, (29) can be expressed as

$$R = x_2 N. \tag{30}$$

Substituting (24) and (30) into (10) yields

$$P_O = \frac{1}{\left(a_1 N^2 + a_2 + a_3/N\right)^2} \tag{31}$$

where

$$a_1 = \frac{\omega}{U_s\sqrt{R_W}}\cdot x_1\left(\Delta,\alpha\right) \tag{32}$$

$$a_2 = \frac{1}{U_s\omega\sqrt{R_W}}\cdot\frac{{x_2}^2}{x_1\left(\Delta,\alpha\right)} \tag{33}$$

$$a_3 = \frac{\sqrt{R_W}}{U_s\omega}\cdot\frac{x_2}{x_1\left(\Delta,\alpha\right)}. \tag{34}$$

By differentiating P_O with respect to N and equating the differential function to zero, the optimum value of N for maximum output power can be obtained as

$$N_{\rm OPT} = \sqrt[3]{\frac{R_W}{2\omega^2}\cdot\frac{x_2}{x_1(\Delta,\alpha)^2}}. \tag{35}$$

When (35) is satisfied, the maximum output power can easily be solved as (36) as shown at the bottom of the page.

Substituting the value of $x_1(0\sim 10\ \text{cm}, 0\sim 50^\circ)$ and other defined parameters into (35) and (36), we can get: $N_{\rm OPT}\asymp 7, \rm P_{O\_MAX}\asymp 101.53\ W$. To verify the calculation results, Fig. 10 depicts the output power curves against spatial misalignments under different coil turns according to (10) when $R_L = 10\ \Omega$. It is observed that the output power reaches maximum value and remains almost constant within the misalignments range of 0∼10 cm and 0∼50° when $N = \rm N_{OPT}$.

$$P_{O\_\rm MAX} = \frac{{U_S}^2}{\left(\sqrt[6]{\frac{R_W}{16\omega^2}\cdot\frac{{x_2}^4}{x_1(\Delta,\alpha)^2}} + \frac{1}{\omega\sqrt{R_W}}\cdot\frac{{x_2}^2}{x_1(\Delta,\alpha)} + \sqrt[6]{\frac{4R_W}{\omega^2}\cdot\frac{{x_2}^4}{x_1(\Delta,\alpha)^2}}\right)^2} \tag{36}$$

TABLE I
PARAMETERS OF THE PROTOTYPE

Parameter		Symbol	Value			
			Original design	After optimization		
				Case 1	Case 2	Case 3
Transmitter	Radius	r_S	11 cm	11 cm	11 cm	11 cm
	Turns	N_S	14	7	14	4
Receiver	Radius	r_D	11 cm	11 cm	11 cm	11 cm
	Turns	N_D	14	7	4	14
Input voltage		V_{in}	24 V			
Operating frequency		f_s	202 kHz			
Transmission distance		d	24 cm			

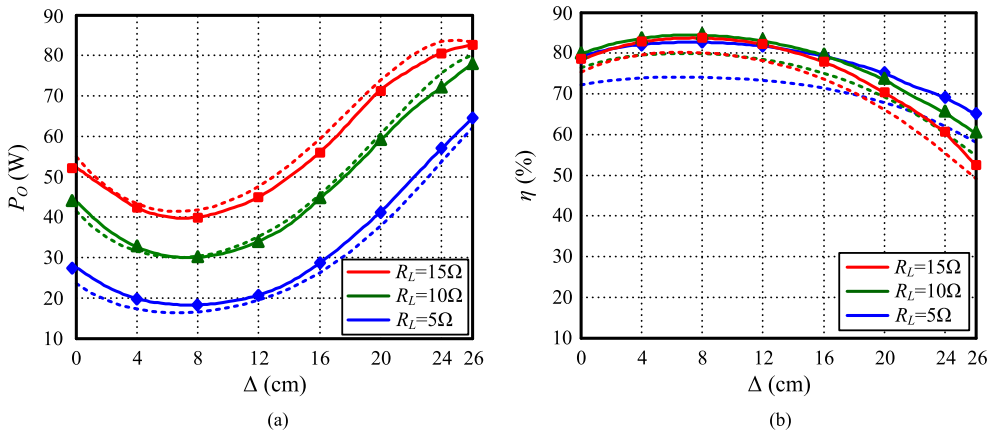

Fig. 12. Transmission characteristics with lateral misalignment when $\alpha = 60°$. (a) Output power. (b) Transmission efficiency.

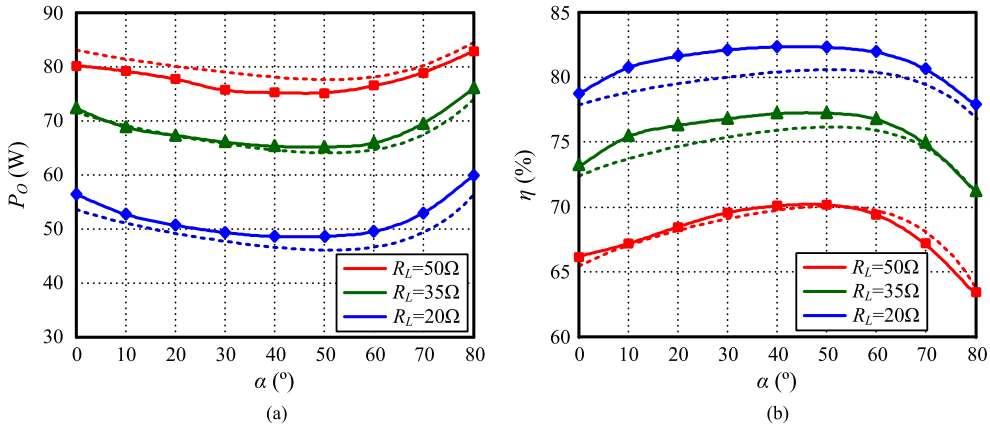

Fig. 13. Transmission characteristics with angular misalignment when $\Delta = 10$ cm. (a) Output power. (b) Transmission efficiency.

V. EXPERIMENTAL VERIFICATIONS

In order to validate the theoretical analysis, a prototype has been built and tested in the laboratory, as shown in Fig. 11. The main specifications and coil parameters before and after optimization are listed in Table I.

Experimental measured data under original design are plotted in Figs. 12 and 13 by solid lines, along with the theoretical curves, given by (10) and (11) in dashed lines. Fig. 12 shows the output power and transmission efficiency with lateral misalignment under different load condition, when $\alpha = 60°$. Fig. 13 depicts the transmission characteristics with angular misalignment under different load condition, when $\Delta = 10$ cm. By contrast with the measured data, it is observed that the experimental results are well in agreement with the theoretical analysis. It should be noted that the efficiency measured in experiments is the transmission efficiency from transmitting coils to receiving coils, only the ac power transfer efficiency. Power losses in half-bridge inverter and voltage-doubler rectifier are not included. The theorectical curve in Fig. 12(a) is different slightly with the curves in Fig. 10(a), for the operation frequency and distance in the theorectical analysis are modified to match the experimental parameters well.

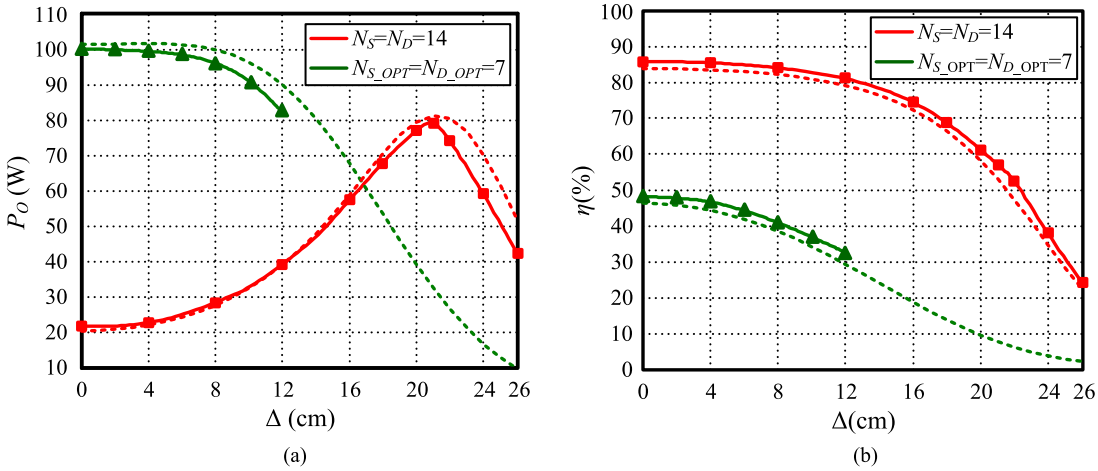

Fig. 14. Measured transmission characteristics with lateral misalignments in case 1. (a) Output power. (b) Transmission efficiency.

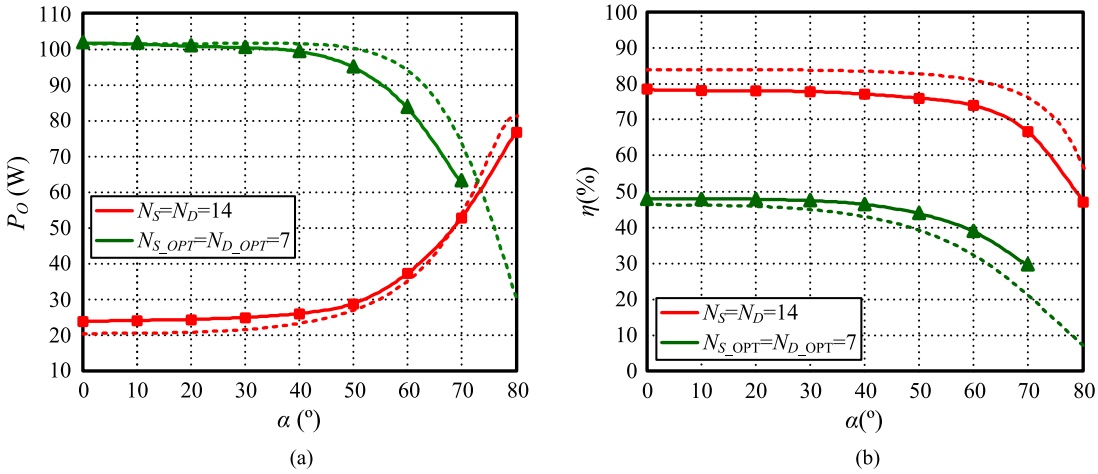

Fig. 15. Measured transmission characteristics with angular misalignments in case 1. (a) Output power. (b) Transmission efficiency.

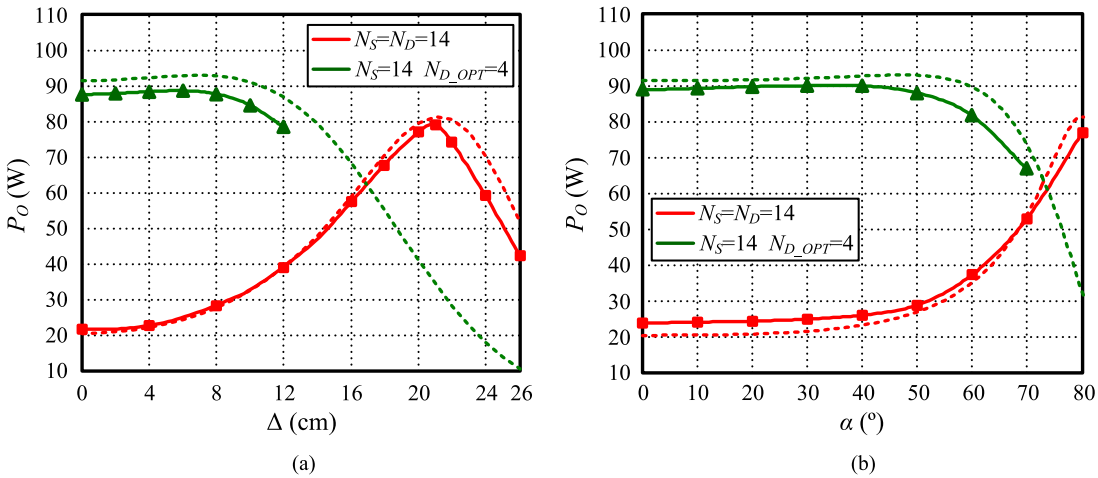

Fig. 16. Measured output power with spatial misalignments in case 2. (a) Lateral misalignment. (b) Angular misalignment.

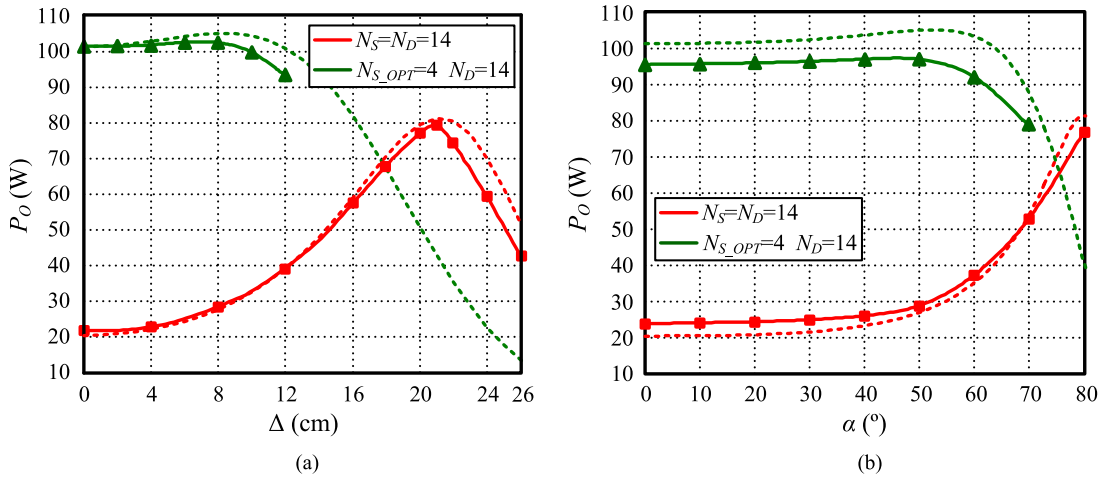

Fig. 17. Measured output power with spatial misalignments in case 3. (a) Lateral misalignment. (b) Angular misalignment.

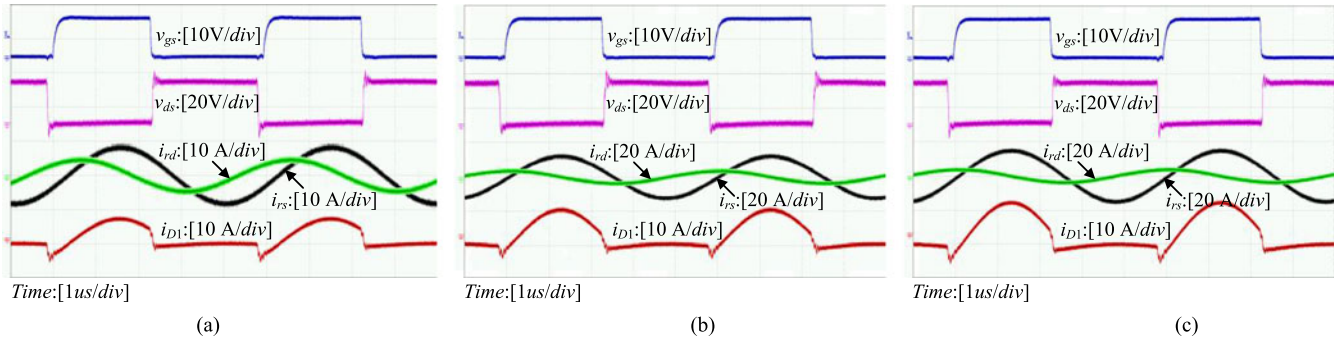

Fig. 18. Experimental waveforms with various spatial scales. (a) Lateral misalignment case ($\Delta = 10$ cm, $\alpha = 0°$). (b) Angular misalignment case ($\Delta = 0$ cm, $\alpha = 30°$). (c) General misalignment case ($\Delta = 10$ cm, $\alpha = 30°$).

Experimental measured data in three optimization cases when $R_L = 10\ \Omega$ are plotted in Figs. 14–17 by solid lines, along with the theoretical curves, given by (10) in dashed lines. As seen in Figs. 14–17, the measured data match well with the theoretical analysis. Besides, after optimization, maximum and nearly stable output power can be achieved within the misalignments range of 0–10 cm and $0 - 50°$, proving the normalization method to be valid for the optimal design of coils. From Figs. 14 and 15, it can be known that the transmission efficiency achieved by the maximum power transfer theorem, which requires impedance matching, cannot exceed 50%. This is an inherent limitation of the maximum power transfer principle for mid-range WPT. Generally, maximum power transfer theorem is used in mid-range applications in which the energy efficiency is not of primary concern. It is suitable for relatively low power applications such as charging of wireless sensor nodes, etc.

Fig. 18 shows the experimental waveforms with three different spatial scales. Fig. 18(a) shows the key experimental waveforms in the lateral misalignment case when $\Delta = 10$ cm. Fig. 18(b) shows the same waveforms in the angular misalignment case when $\alpha = 30°$. Fig. 18(c) depicts the corresponding waveforms in the general case when $\Delta = 10$ cm and $\alpha = 30°$. As shown in Fig. 18, before the switch turns on, the drain current i_D is negative, which indicates that the parasitic diode of the switch has conducted. In the meantime, the drain-to-source voltage $v_{\rm ds}$ was clamped to zero. So, the switches can achieve ZVS. Besides, it can be observed that two resonant currents are both good sinusoidal waveforms, and the phase difference between them is about 90°.

VI. Conclusion

This paper proposed an intensive analytical model for the MCR WPT system. Based on the equivalent circuit model and FHA method, transmission characteristics of the system were analyzed in detail. The mutual inductance formulas in arbitrary spatial scales were deduced with mathematical methods. So, the relationship among the output power, transmission efficiency, and spatial scales can be obtained apparently. Research results show that the mutual inductance varies with the spatial scales, which further causes fluctuations in output power and transmission efficiency. For a fixed load resistance, there is a corresponding mutual inductance that can achieve the maximum output power. While the transmission efficiency decreases as the mutual inductance reduces. By normalizing the mutual inductance formula and solving the output power differential equation, steady operation range and optimum value of coil turns were easily obtained. Research results show that after the optimal design of coil parameters, maximum and nearly stable output power can be achieved within the predicable misalign-

ments range. Beyond this range, the output power will decrease sharply with the increasing lateral or angular misalignment. A prototype was built and tested to validate the theoretical analysis. The experimental results are well in agreement with the theoretical analysis, verifying the accuracy of the analytical model and the feasibility of the proposed optimization method.

REFERENCES

[1] C. K. Lee, W. X. Zhong, and S. Y. R. Hui, "Recent progress in mid-range wireless power transfer," in *Proc. IEEE Energy Convers. Congr. Expo.*, 2012, pp. 3819–3824.

[2] N. Shinohara, "Wireless power transmission progress for electric vehicle in Japan," in *Proc. IEEE Radio Wireless Symp.*, 2013, pp. 109–111.

[3] S. Y. R. Hui and W. W. C. Ho, "A new generation of universal contactless battery charging platform for portable consumer electronic equipment," *IEEE Trans. Power Electron.*, vol. 20, no. 3, pp. 620–627, May 2005.

[4] H. G. Lim, Y. H. Yoon, C. W. Lee, I. Y. Park, B. S. Song, and J. H. Cho, "Implementation of a transcutaneous charger for fully implantable middle ear hearing device," in *Proc. IEEE Conf. Eng. Med. Biol. Soc.*, 2005, pp. 6813–6816.

[5] S. Y. R. Hui, W. X. Zhong, and C. K. Lee, "A critical review on recent progress in mid-range wireless power transfer," *IEEE Trans. Power Electron.*, vol. 29, no. 9, pp. 4500–4511, Sep. 2014.

[6] M. G. Egan, D. L. O'Sullivan, J. G. Hayes, M. J. Willers, and C. P. Henze, "Power-factor-corrected single-stage inductive charger for electric vehicle batteries," *IEEE Trans. Ind. Electron.*, vol. 54, no. 2, pp. 1217–1226, Apr. 2007.

[7] A. Kurs, A. Karalis, R. Moffatt, J. D. Joannopoulos, P. Fisher, and M. Soljacic, "Wireless power transfer via strongly coupled magnetic resonances," *Science*, vol. 317, no. 5834, pp. 83–86, Jul. 2007.

[8] X. Zhang and J. Chae, "Working distance comparison of inductive and electromagnetic couplings for wireless and passive underwater monitoring system of rinsing process in semiconductor facilities," *IEEE Sens. J.*, vol. 11, no. 11, pp. 2932–2939, May 2011.

[9] J. W. Kim, H. C. Son, K. H. Kim, and Y. J. Park, "Efficiency analysis of magnetic resonance wireless power transfer with intermediate resonant coil," *IEEE Antennas Wireless Propag. Lett.*, vol. 10, pp. 389–392, May 2011.

[10] T. Hosotani and I. Awai, "A novel analysis of ZVS wireless power transfer system using coupled resonators," in *Proc. IEEE Microw. Workshop Series*, 2012, pp. 235–238.

[11] O. Jonah, S. V. Georgakopoulos, and M. M. Tentzeris, "Orientation insensitive power transfer by magnetic resonance for mobile devices," in *Proc. IEEE Wireless Power Transfer*, 2013, pp. 5–8.

[12] S. Babic and C. Akyel, "Calculating mutual inductance between circular coils with inclined axes in air," *IEEE Trans. Magn.*, vol. 44, no. 7, pp. 1743–1750, Jul. 2008.

[13] Z. G. Dang and J. A. A. Qahouq, "Modeling and investigation of magnetic resonance coupled wireless power transfer system with lateral misalignment," in *Proc. IEEE Appl. Power Electron. Conf.*, 2014, pp. 1317–1322.

[14] J. H. Wang *et al.*, "Lateral and angular misalignments analysis of a new PCB circular spiral resonant wireless charger," *IEEE Trans. Magn.*, vol. 48, no. 11, pp. 4522–4525, Nov. 2012.

[15] K. Fotopoulou and B. W. Flynn, "Wireless power transfer in loosely coupled links: Coil misalignment model," *IEEE Trans. Magn.*, vol. 47, no. 2, pp. 416–430, Feb. 2011.

[16] L. Gao *et al.*, "Optimum design of coil for wireless energy transmission system based on resonant coupling," in *Proc. IEEE Int. Conf. Control Autom.*, 2013, pp. 190–195.

[17] H. C. Li, K. P. Wang, L. Huang, J. Li, and X. Yang, "Coil structure optimization method for improving coupling coefficient of wireless power transfer," in *Proc. IEEE Appl. Power Electron. Conf.*, 2015, pp. 2518–2521.

[18] J. H. Wang *et al.*, "Analytical design study of a novel Witricity charger with lateral and angular misalignments for efficient wireless energy transmission," *IEEE Trans. Magn.*, vol. 47, no. 10, pp. 2616–2619, Oct. 2011.

[19] H. C. Li, J. Li, K. P. Wang, W. J. Chen, and X. Yang, "A maximum efficiency point tracking control scheme for wireless power transfer systems using magnetic resonant coupling," *IEEE Trans. Power Electron.*, vol. 30, no. 7, pp. 3998–4008, Aug. 2014.

Fuxin Liu (S'04–M'09–SM'16) was born in Heilongjiang Province, China, in 1979. He received the B.S., M.S., and Ph.D. degrees in electrical engineering from the Nanjing University of Aeronautics and Astronautics (NUAA), Nanjing, China, in 2001, 2004, and 2007, respectively.

In 2007, he joined the Faculty of the College of Automation Engineering, NUAA, where he is currently an Associate Professor. His main research interests include soft-switching dc/dc converters, wireless power transfer, and renewable energy generation systems.

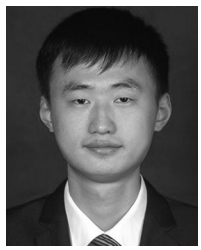

Yong Yang was born in Jiangsu Province, China, in 1993. He received the B.S. degree in electrical engineering and automation from the Nanjing University of Aeronautics and Astronautics, Nanjing, China, in 2015, where he is currently working toward the M.S. degree in electrical engineering.

His main research interests include wireless power transfer.

Dan Jiang was born in Jiangsu Province, China, in 1992. She received the B.S. and M.S. degrees in electrical engineering from the Nanjing University of Aeronautics and Astronautics, Nanjing, China, in 2013 and 2016, respectively.

In 2016, she joined Monolithic Power Systems, Hangzhou, China. Her main research interests include wireless power transfer.

Xinbo Ruan (M'97–SM'02–F'16) received the B.S. and Ph.D. degrees in electrical engineering from the Nanjing University of Aeronautics and Astronautics (NUAA), Nanjing, China, in 1991 and 1996, respectively.

In 1996, he joined the College of Automation Engineering, NUAA, where he became a Professor in 2002. In 2008–2011, he was also with the College of Electrical and Electronic Engineering, Huazhong University of Science and Technology, China. He is the author or coauthor of seven books and more than 200 technical papers published in journals and conferences. His main research interests include soft-switching power electronics converters, power electronics system integration and renewable energy generation system.

Dr. Ruan currently serves as an Associate Editor for the IEEE TRANSACTIONS ON INDUSTRIAL ELECTRONICS, the IEEE JOURNAL OF EMERGING AND SELECTED TOPICS ON POWER ELECTRONICS, the IEEE TRANSACTIONS ON POWER ELECTRONICS, and the IEEE TRANSACTIONS ON CIRCUITS AND SYSTEMS-II. From 2005 to 2013, he served as Vice President of the China Power Supply Society.

Xuling Chen (S'14) was born in Hunan Province, China, in 1979. She received the B.S., M.S., and Ph.D. degrees in mechanical and electrical engineering from the Nanjing University of Aeronautics and Astronautics (NUAA), Nanjing, China, in 2002, 2005, and 2011, respectively.

In 2005, she joined the Faculty of the College of Mechanical and Electric Engineering, NUAA, where she is currently a Lecturer. Her main research interests include wireless power transfer, mechanical and electrical engineering, and mechanical design.